Editors' Suggestion | Featured in Physics

Atomic Step Flow on a Nanofacet

Jean-Christophe Harmand,[1,*] Gilles Patriarche,[1] Frank Glas,[1] Federico Panciera,[1] Ileana Florea,[2] Jean-Luc Maurice,[2] Laurent Travers,[1] and Yannick Ollivier[1]

[1]*Centre de Nanosciences et de Nanotechnologies, CNRS, Université Paris-Sud, Université Paris-Saclay, Avenue de la Vauve, 91120 Palaiseau, France*

[2]*Laboratoire de Physique des Interfaces et des Couches Minces, Ecole polytechnique, CNRS, Université Paris-Saclay, 91128 Palaiseau, France*

(Received 26 April 2018; revised manuscript received 14 July 2018; published 19 October 2018)

Crystal growth often proceeds by atomic step flow. When the surface area available for growth is limited, the nucleation and progression of the steps can be affected. This issue is particularly relevant to the formation of nanocrystals. We examine the case of Au-catalyzed GaAs nanowires, which we grow in a transmission electron microscope. Our *in situ* observations show that atomic layers nucleate at the periphery of the interface between the nanowire and the catalyst droplet. From this starting location, the atomic step flows within a restricted area of hexagonal shape. At specific partial coverages, the monolayer configuration changes abruptly. A simple model based on the geometry of the system and its edge energies explains these observations. In particular, we observe an inversion of the step curvature which reveals that the effective energy per unit length of monolayer edge is much lower at the interface periphery than inside the catalyst droplet.

DOI: 10.1103/PhysRevLett.121.166101

Harnessing the potential of nanocrystals for a wide range of applications requires an ever-improved control of their properties. A remarkable specificity of nanocrystals is the strong influence of their surfaces and edges on their properties. The important role of crystal boundaries also manifests itself at the growth stage. Indeed, surfaces influence the morphology and crystalline arrangement of nanostructures, not only as regards thermodynamics but also via their growth dynamics. This is notably illustrated in the vapor-liquid-solid (VLS) growth [1] of semiconductor nanowires (NWs). In this method, vapor containing the NW constituents is supplied to a liquid catalyst nanoparticle. Upon supersaturation of the catalyst droplet, crystallization occurs: A nanocrystal forms, one of its facets in contact with the droplet. This nanofacet is where crystal growth further proceeds. A detailed and real-time observation of the liquid-solid interface is thus expected to clarify the role of the boundaries in the crystallization process.

Pioneering studies based on *in situ* NW growth in a transmission electron microscope (TEM) have already reported such observations. It was clearly shown that the atomic layers form sequentially at the catalyst-NW interface [2–5]. In some cases, the propagation along the interface of the atomic step bordering the layer could even be seen [3,5]. In planar growth of macroscopic crystals from a vapor, the step flow regime has been studied for several decades [6–8]. This growth mode results from the preferential attachment of atoms to the steps present on a crystalline surface. When adatom diffusion is sufficient, this regime prevails over the formation of new nuclei onto flat terraces. In the NW case, the area where growth takes place is so small that it is traversed by single steps which flow one by one. However, the precise geometry and dynamics of this interfacial step flow remain to be explored. In the present work, we demonstrate that the NW boundaries have a direct impact on the geometry of the step motion. This allows us to evaluate the capillary forces acting on the growing system. Together with the location of the first observable islands, these results provide robust and quantitative arguments to explain the formation of a metastable crystalline phase.

Indeed, compound semiconductor NWs grow mostly along the $\langle 111 \rangle$ or $\langle 0001 \rangle$ directions [2–5], these indexings referring to the zinc blende (ZB) or wurtzite (WZ) structures that the NW can adopt [9]. The conditions determining which of these two phases forms have been much discussed [5,10–12], but experimental support is still necessary to clarify this question. For many III-V compounds, the stable bulk crystal phase is ZB. In 2007, we proposed that the crystalline stacking of each monolayer (ML) [13] is determined at its nucleation stage and that WZ stacking is related to nucleation at the triple phase line (TPL), the boundary between NW, catalyst, and vapor: With this anchor to the TPL, the total edge energy of the ML nucleus can be lower in WZ position than in ZB position [11]. Hence, identification of the exact nucleation site is key to understanding the mechanisms of phase selection in NW growth.

To date, full experimental evidence of MLs forming at the TPL is lacking. Some TEM observations of *in situ* NW growth suggest that it is the case [2,5]. Nevertheless, the observation conditions adopted in these studies, with the

electron beam parallel to the LS interface, provide an incomplete picture of ML formation and progression. Here, we present in addition bird's eye views of growing NWs which reveal essential complementary information. A two-dimensional projection of the growing ML is visualized, from the early stage of formation to ML completion. We confirm that WZ layers start from the periphery of the NW top facet, and we image, analyze, and model the progression of the step within this hexagonal perimeter. Relevant edge energies are extracted. This leads to a better understanding of the formation of the nanocrystal and ultimately to a better control of its structure.

We observe the VLS growth of GaAs NWs in real time. We use a modified FEI environmental TEM equipped with an image aberration corrector. Two ports were designed to implement Ga and As_4 molecular beam sources in the TEM. NW formation is catalyzed by Au particles dispersed on a heating carrier membrane, and *in situ* growth is performed by molecular beam epitaxy at 400 °C. At this temperature, the Au particles alloy with Ga to form liquid droplets. Upon As supersaturation of the droplets, GaAs NWs of hexagonal shape crystallize under the droplets. The boundaries of this system consist of the NW-catalyst interface, the NW sidewalls, and the surface of the liquid catalyst particle. We examine the formation of the WZ phase. The sidewalls of the NWs are $\{11\bar{2}0\}$ facets, and the hexagon sides are $\langle 10\bar{1}0\rangle$ directions. We first present an atomically resolved growth observation in a $\langle 11\bar{2}0\rangle$ zone axis. The electron beam is then parallel to the LS interface, and the atomic columns parallel to the beam produce a strong contrast (Fig. 1).

The liquid-solid interface is atomically flat, except when a ML forms. When this happens, a single atomic step flows apparently from one NW edge to the opposite (Video SV1 [14]). We never see two steps progressing at the same time. This conforms to the *mononuclear* regime [15], whereby each ML forms from a single nucleus and is completed before the next nucleation event, and also to previous observations [2,3,5]. Though highly resolved, this cross-sectional view gives only a one-dimensional projection of the ML advance, and the lateral geometry of its edge remains unknown. The step motion seems to alternate between left to right and right to left (to be discussed later), but where each ML starts and ends is not identified precisely. The MLs seem to nucleate at the TPL, but this cannot be ascertained, and the time needed to complete a ML cannot be established unambiguously.

To clarify these questions, we carried out observations with the NW axis titled slightly off a zone axis. Then, the resolution is degraded, but the liquid-solid interface is seen as a two-dimensional projection. We chose a tilt angle of about 10° as a good compromise, ensuring that the projected interface has a significant area while a good contrast is maintained when a single III-V biatomic step flows at this interface (Fig. 2 and Videos SV2 and SV3 [14]). By observing afterwards the same portion of the NW in a zone-axis orientation, we checked that its structure is indeed WZ. In such bird's eye views, the hexagonal shape of the NW periphery can now be figured out, and the various portions of the step edge can be indexed precisely. We determine the polar angles of the interface projection plane by fitting the three $\langle 10\bar{1}0\rangle$ directions of the sides of the hexagon constituting the TPL. Three other low-index directions, the $\langle 11\bar{2}0\rangle$ axes, are projected in this plane in order to index precisely the step edges. We now examine the nucleation and subsequent expansion of the ML.

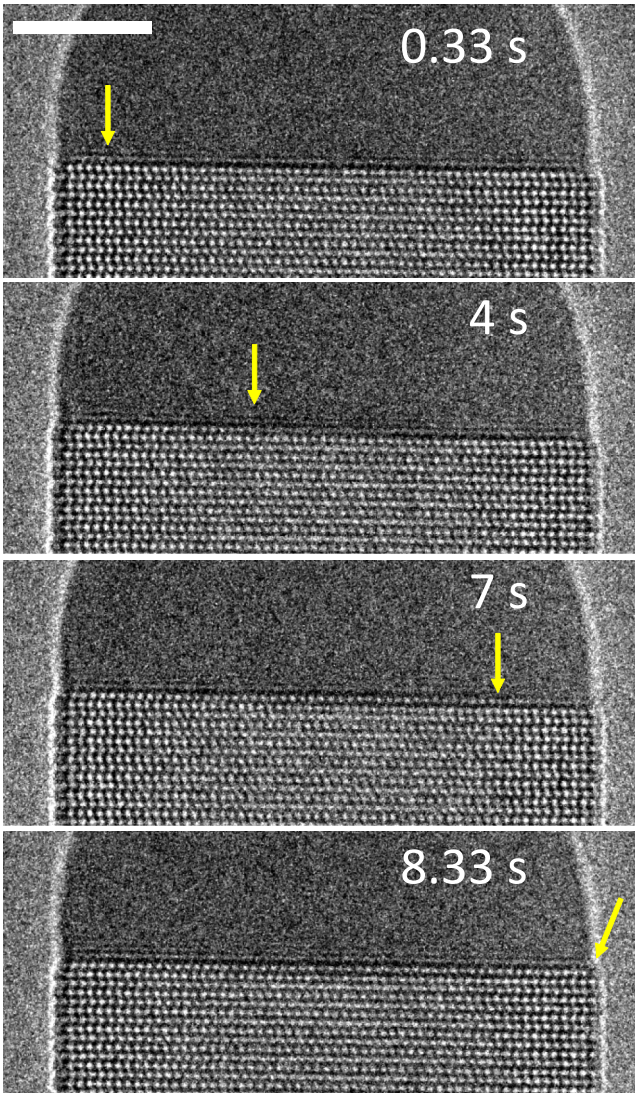

FIG. 1. Images from Video SV1 [14] showing the flow of a single ML step (arrows) during the growth of a GaAs NW with wurtzite structure. Scale bar, 5 nm.

The nucleation event giving rise to each ML is too elusive to be directly observed: The critical nucleus likely consists of only a few III-V pairs and, being unstable, expands very rapidly beyond the critical size by collecting atoms from the liquid phase. For each ML, the smallest island visualized occupies about 10% of the top facet. It is systematically anchored to the TPL and actually to a corner

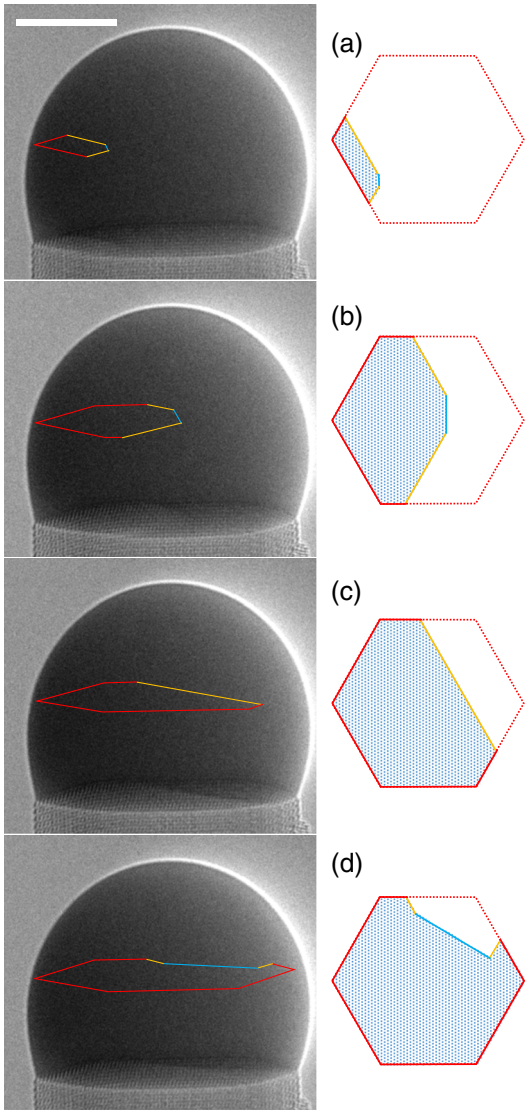

FIG. 2. Left: Bird's eye views of a GaAs ML progressing at the liquid-solid interface, showing different successive configurations of the step edge (images extracted from Video SV2 [14]). The contour of the growing layer is schematically reproduced above the interface in color: red for the NW periphery and yellow and blue for step edges along the $\langle 10\bar{1}0\rangle$ and $\langle 11\bar{2}0\rangle$ directions. Right: Normal projection of each configuration. Note the change of concavity at high coverage. Scale bar, 10 nm.

of the hexagon [Fig. 2(a); apart from the TPL portion, the ML edge consists of two $\langle 10\bar{1}0\rangle$ branches, with possibly a short $\langle 11\bar{2}0\rangle$ truncation]. This implies that nucleation occurs either at the TPL or away from the TPL but somewhere within the total area covered by such islands. For ideal rhombic-shaped islands, this area is a fraction $f \approx 0.60$ of the top facet area. Let us assume a probability $P \leq 1$ for nucleation at the TPL and a uniform nucleation probability away from the TPL. Then, the probability of n such observations is $[P + f(1-P)]^n$. We observed more than 50 MLs, all starting in this fashion. The probability

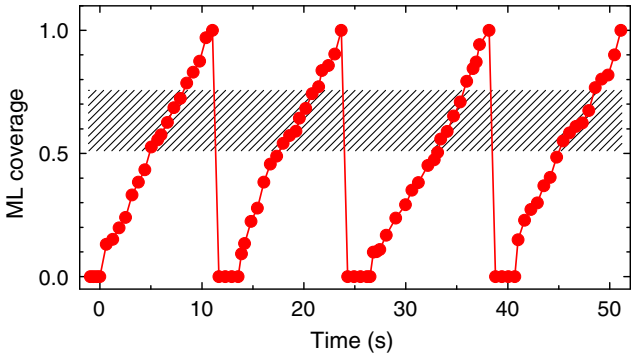

FIG. 3. ML coverage as a function of time for the four MLs of Video SV2 [14]. The concavity of each partial ML changes at coverages within the hatched zone.

of such a series is appreciable only if P is very close to 1: For instance, it is 0.015 for $P = 0.8$ and still only 0.364 for $P = 0.95$. This makes systematic nucleation at the TPL very likely.

In our growth conditions, the amount of As in the liquid is very small. The ML size after nucleation and fast initial expansion can be assimilated to the stopping size introduced by Dubrovskii [16]. The ML then extends more slowly as droplet refills from the external fluxes (Fig. 3). This allows us to track its geometry in detail. As the facet coverage increases, the initial convex step edge geometry is first conserved, the ML bordering successively three and four sides of the top facet [Fig. 2(b)]. When the coverage exceeds about 0.5, the configuration changes abruptly. The ML now borders five sides of the hexagon, three of them fully occupied, and the internal step edge becomes a single straight $\langle 10\bar{1}0\rangle$ segment [Fig. 2(c)]. It retains this geometry up to a coverage of about 0.75. It then shifts to a concave configuration, combining $\langle 11\bar{2}0\rangle$ and $\langle 10\bar{1}0\rangle$ segments, and its total length decreases [Fig. 2(d)] until ML completion.

These observations can be explained by modeling the extension of each ML as follows. In line with the experiments, the incomplete ML is assumed to be bounded by a step edge composed of three types of segments, lying either at the TPL (along $\langle 10\bar{1}0\rangle$, index $i = 0$) or at the liquid-solid interface away from the TPL, in which case the segment may be along either $\langle 10\bar{1}0\rangle$ ($i = 1$) or $\langle 11\bar{2}0\rangle$ ($i = 2$). We attribute to these segments different energies per unit length γ_i. We consider 31 possible step configurations, defined by the number and sequence of such segments. The total step energy is $W_s = \sum_p L_p \gamma_{i(p)}$, where the summation extends over all segments p, of type $i(p)$ and length L_p. For each ML coverage, we select the configuration of minimal energy.

This simple procedure captures remarkably well the experimental sequence of step geometry and the coverages θ at which the transitions between configurations occur (Fig. 4). It also yields precise information about the relative values of the step energies γ_i. Indeed, the match is achieved only if the energies of the two segments at the LS

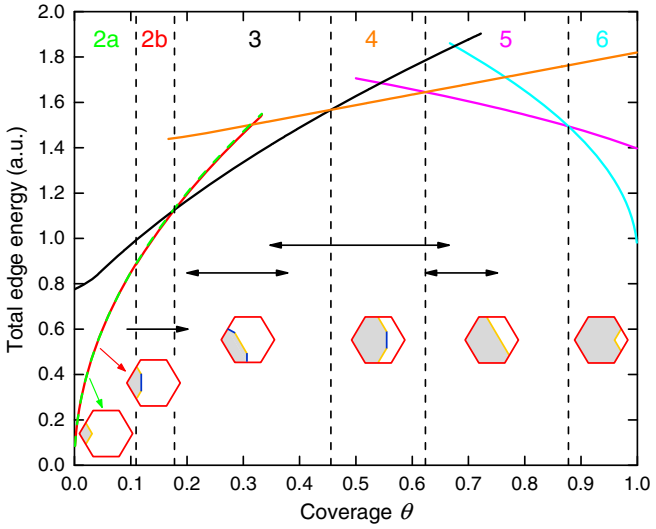

FIG. 4. Variation with ML coverage of the total energies of the various step configurations predicted to occur (and schematized at the bottom), calculated with optimized step energies. Dashed lines mark the shifts between configurations and arrows the ranges of coverage where these are experimentally observed. The successive configurations involve increasing numbers of hexagon sides bordered by the ML (indicated at top), except the first two.

interface are close but slightly lower for the $\langle 10\bar{1}0\rangle$ direction (as expected from its experimental dominance), namely, $\gamma_2/\gamma_1 = 1.05 \pm 0.01$. Conversely, the energy of the segment at the TPL must be much lower: Only a ratio $\gamma_0/\gamma_1 = 0.25 \pm 0.05$ allows one to reproduce the present observations.

While the precise sequence of step configurations varies slightly from one experiment to another, the change of concavity [e.g., from Figs. 2(b) to 2(d)] is systematically observed. This is directly related to a much lower energy for the portion of the step at the TPL. In turn, this lends strong support to the mechanism that we proposed for WZ formation in NWs: WZ can form only if the layer nucleates at the TPL, and TPL nucleation may be energetically very favorable because forming a portion of step there suppresses part of the liquid-vapor interface [11]. For the same reason, it is favorable to add material to the ML at the TPL rather than at an edge internal to the droplet. This is, of course, balanced by a tendency to reduce the total ML perimeter at a given coverage, leading to initial convex configurations. This general confirmation of our model can be pursued quantitatively. In the terms of this model, the specific energies defined here are written $\gamma_0 = h(\gamma_{nV} - \gamma_{LV}\sin\beta_e)$ and $\gamma_1 \approx h\gamma_{nL}$, where γ_{nV} and γ_{nL} are the energies per unit area of the lateral nucleus-vapor and nucleus-liquid interfaces, respectively, γ_{LV} that of the liquid-vapor interface, β_e the experiment-dependent contact angle of the droplet on the NW top facet, and h the ML height. Recall that only one γ_{nL} energy is considered in Ref. [11], which we assimilate here, e.g., to γ_1, given that $\gamma_1 \approx \gamma_2$. Hence, $\gamma_{nL} = (\gamma_{nV} - \gamma_{LV}\sin\beta_e)/f$ with $f = \gamma_0/\gamma_1$. Energy γ_{LV} depends on the unknown composition of the surface of the Au-Ga droplet. However, with $\gamma_{nV} = 0.70\ \mathrm{J\,m^{-2}}$ (the $\{11\bar{2}0\}$ sidewall energy calculated in Ref. [17]), $\beta_e = 110°$ (as measured in the present experiment), and $f = 0.25$ (obtained by fitting the modeled configuration sequence to the experiment), a positive γ_{nL} is found only if γ_{LV} is very close to the surface tension of pure Ga ($0.69\ \mathrm{J\,m^{-2}}$ at the growth temperature [18]). This strongly suggests that Ga segregates at the droplet surface. Assuming a pure Ga droplet surface yields the largest γ_{nL}, namely, $0.20\ \mathrm{J\,m^{-2}}$, a value only slightly larger than our experimental determination in the case of a pure Ga droplet ($0.123\ \mathrm{J\,m^{-2}}$) [19]. Moreover, Ref. [11] predicts that nucleation at the TPL is favored for contact angles in an interval $[\pi - \beta_c, \beta_c]$ with the critical angle β_c given by

$$\gamma_{nV} - \gamma_{nL} - \gamma_{LV}\sin\beta_c = 0.$$

Hence, β_c can be evaluated from our experiments via the formula $\sin\beta_c = [\sin\beta_e - (1-f)\gamma_{nV}/\gamma_{LV}]/f$. For the range of admissible values of γ_{LV}, this yields a critical angle β_c between 120° and 134°, which compares well with the experimental critical angle (around 121°) for the ZB-WZ transition.

Figure 3 shows that coverage θ increases almost linearly with time, with slight and random deviations. In this particular experiment, the average step flow lasts about 10 s per ML. A mean time of 2.7 s separates the completion of a ML from the nucleation of the following one. This nonzero waiting time indicates that a nucleation barrier must be overcome before forming a critical nucleus. In cross-sectional views such as Video SV1 [14], the partial vision of the ML progression leads one to largely overestimate this waiting time.

The question of where successive layers nucleate remains to be clarified. In Video SV2 [14], four consecutive MLs all nucleate near the same corner. In contrast, Video SV3 [14] shows two alternating nucleation sites for a sequence of eight MLs. Though not perfect, this alternation is quite surprising. A small asymmetry of the NW cross section could be responsible for it. If, for instance, the sides of the hexagonal periphery have slightly different lengths, the shape of the droplet and its contact angle will be asymmetric [20]. Hence, the nucleation barrier could vary along the TPL, some corners being more favorable than others. In addition, the top facet of a WZ NW with six ideal $\{11\bar{2}0\}$ sidewalls presents two types of chemically nonequivalent corners, which alternate along the hexagonal periphery and swap type at each ML. An asymmetry of the NW cross section combined with one type of corner being more favorable than the other for nucleation could explain why sometimes layers form alternatively from two distinct corners of the TPL.

In our GaAs NWs, WZ stacking prevails for contact angles of the Au-Ga catalyst droplet below ~121°, a critical value very similar to that reported in Ref. [5]. Beyond this angle, ZB dominates. We do not discuss here the growth of this latter phase. Suffice to mention that, as other authors [5], we observe that ZB formation in NWs involves very different mechanisms.

Last, we comment on the possible effect of the high-energy electron beam on the growth process. Various electron beam current densities were tested on single NWs observed at a high resolution. Above a few thousands of electrons $Å^{-2}\,s^{-1}$, local heating was evidenced by a rapid deflation of the catalyst droplet. Below 10^3 $Å^{-2}\,s^{-1}$, the range used for the present experiments, this effect was not noticed, and, as long as the contrast was sufficient to observe the step flow, its geometry was found independent of the electron dose. In addition, the postgrowth morphologies of NWs grown under or outside the electron beam were found to be very similar.

Summarizing the formation of a WZ ML in a VLS-grown GaAs NW, we have evidenced that it involves nucleation at the TPL and inversion of the step edge curvature beyond a coverage around 0.5–0.75. These two features reveal that the effective edge energy per unit length is much lower at the TPL than at the step progressing in the liquid. Modeling the change of curvature, we infer that the ratio of these two edge energies is close to 0.25 in our conditions. This is due to the fact that the part of the solid island which borders the TPL replaces the corresponding liquid surface element, reducing significantly its formation energy. This energy depends on the contact angle of the catalyst droplet. At a critical angle near 121°, we observe experimentally a transition from WZ to ZB stacking. This strongly supports the idea [11] that crystal phase selection is directly linked to the site of nucleation, WZ nuclei at the TPL, and ZB nuclei fully immersed in the liquid [21].

We acknowledge Odile Stéphan, leader of TEMPOS (Transmission Electron Microscopy at Palaiseau-Orsay-Saclay), for her continuous support to the NANOMAX project and "Agence Nationale de la Recherche", the French funding agency, in the framework of "Equipements d'excellence" Project No. 10-EQPX-0050.

*Corresponding author.
jean-christophe.harmand@c2n.upsaclay.fr

[1] R. S. Wagner and W. C. Ellis, Appl. Phys. Lett. **4**, 89 (1964).
[2] C.-Y. Wen, M. C. Reuter, J. Tersoff, E. A. Stach, and F. M. Ross, Nano Lett. **10**, 514 (2010).
[3] C.-Y. Wen, J. Tersoff, M. C. Reuter, E. A. Stach, and F. M. Ross, Phys. Rev. Lett. **105**, 195502 (2010).
[4] A. D. Gamalski, C. Ducati, and S. Hofmann, J. Phys. Chem. C **115**, 4413 (2011).
[5] D. Jacobsson, F. Panciera, J. Tersoff, M. C. Reuter, S. Lehmann, S. Hofmann, K. A. Dick, and F. M. Ross, Nature (London) **531**, 317 (2016).
[6] N. Osakabe, Y. Tanishiro, K. Yagi, and G. Honjo, Surf. Sci. **109**, 353 (1981).
[7] R. M. Tromp and M. C. Reuter, Phys. Rev. Lett. **68**, 954 (1992).
[8] S. Tsukamoto, M. Pristovsek, A. Ohtake, B. G. Orr, G. R. Bell, T. Ohno, and N. Koguchi, J. Cryst. Growth **251**, 46 (2003).
[9] M. Koguchi, H. Kakibayashi, M. Yazawa, K. Hiruma, and T. Katsuyama, Jpn. J. Appl. Phys. **31**, 2061 (1992).
[10] T. Akiyama, K. Sano, K. Nakamura, and T. Ito, Jpn. J. Appl. Phys. **45**, L275 (2006).
[11] F. Glas, J.-C. Harmand, and G. Patriarche, Phys. Rev. Lett. **99**, 146101 (2007).
[12] R. E. Algra, V. Vonk, D. Wermeille, W. J. Szweryn, M. A. Verheijen, W. J. P. van Enckevort, A. A. C. Bode, W. L. Noorduin, E. Tancini, A. E. F. de Jong, E. P. A. M. Bakkers, and E. Vlieg, Nano Lett. **11**, 44 (2011).
[13] For a III-V compound, we call *monolayer* the thinnest layer made of equal numbers of group III and group V atoms, namely, a group III plane associated with a neighbor group V plane.
[14] See Supplemental Material at http://link.aps.org/supplemental/10.1103/PhysRevLett.121.166101 for Video SV1: Cross-section view along a $\langle 11\bar{2}0\rangle$ zone axis of Au-catalyzed GaAs NW growth with WZ stacking. Video SV2: Bird's eye view of Au-catalyzed GaAs NW growth with WZ stacking. Formation and progression of 4 consecutive MLs, all starting from the same corner of the hexagonal interface. Video SV3: Bird's eye view of Au-catalyzed GaAs NW growth with WZ stacking. Formation and progression of 8 consecutive MLs starting alternatively from two opposite corners.
[15] D. Kashchiev, *Nucleation: Basic Theory with Applications* (Butterworth-Heinemann, Oxford, 2000).
[16] V. G. Dubrovskii, Cryst. Growth Des. **17**, 2589 (2017).
[17] V. Pankoke, P. Kratzer, and S. Sakong, Phys. Rev. B **84**, 075455 (2011).
[18] S. C. Hardy, J. Cryst. Growth **71**, 602 (1985).
[19] F. Glas, M. R. Ramdani, G. Patriarche, and J.-C. Harmand, Phys. Rev. B **88**, 195304 (2013).
[20] N. Jiang, J. Wong-Leung, H. J. Joyce, Q. Gao, H. H. Tan, and C. Jagadish, Nano Lett. **14**, 5865 (2014).
[21] V. G. Dubrovskii, N. V. Sibirev, J.-C. Harmand, and F. Glas, Phys. Rev. B **78**, 235301 (2008).